Title: Connecting visual perception with proton therapy-induced optic damage using archetypal analysis

Authors

Thao-Nguyen Pham[1], Thibaud Mathis[2], Nathan Azemar[3], Mathieu Seraphim[1], Cyril Moignier [4], Jean-Claude Quintyn[5], Juliette Thariat[1,2]

Institutions

[1] Department of Radiation Oncology, Centre François Baclesse, Caen, Normandy

[2] Service d'Ophtalmologie, Hôpital de La Croix-Rousse, Hospices Civils de Lyon, 69004 Lyon, France

[3] Laboratoire de physique corpusculaire UMR6534 IN2P3/ENSICAEN, Université de Caen- Normandie

[4] Medical Physics Department, Centre François Baclesse, Caen, France

[5] Department of Ophthalmology, University Hospital, Caen, Normandy

Funding: Funding includes PMRT ERDF-FSE 2014-2020 (Grant No. 18P03532/18 E01765), SEQ-RTH22 (Subvention No. 2023-017 from INCa) for voxel-based analysis of toxicities, and the PTCOG Research Grant 2024 for Medicine.

Ethics statement: Institutional Review Board (IRB) approval was obtained, and all patients provided informed consent.

Abstract

Purpose: Radiotherapy can lead to radiation-induced optic neuropathy (RION), with vision loss and visual field deficits related to localized damage to the optic pathways. Accurately quantifying visual field deficits and establishing their spatial relationship with anatomical structures and radiation dose distribution remains a significant challenge. We applied archetypal analysis of visual fields as a novel artificial intelligence approach in oncology to identify distinct, interpretable patterns of visual field loss and to model their spatial evolution over time after pencil beam scanning proton therapy.

Methods: Machine learning of standardized automated static visual field perimetry was used to decompose the high-dimensional visual field data into convex combinations of representative visual loss patterns, i.e. visual archetypes, at both the eye and patient levels. Associations between archetype proportions and radiation dose metrics were evaluated using linear regression, stratified by baseline visual field to account for pre-existing deficits.

Results: In 236 patients, 7 archetypal patterns of visual field loss were identified, including tunnel vision, temporal hemianopia, and diffuse full-field loss. More severe patterns were more frequently observed in patients with meningiomas and pituitary adenomas. Longitudinal analysis revealed an annual reduction of 1.9% in the normal visual field archetype in patients with no-to-mild baseline deficits and 9.7% in those with moderate deficits. Dose-archetype associations were clinically significant after adjusting for baseline deficits. Each 1 Gy increase in minimum chiasm dose was associated with a 0.2% decrease in the normal vision archetype.

Conclusion: This is the first application of archetypal analysis for predicting RION. It enables spatially grounded reconnection between patient perception and radiation damage along optic pathways. This approach offers new mechanistic insights into optic pathway injury towards voxel-level correlation between radiation dose and functional loss and supports data-driven personalization of radiotherapy.

Keywords: archetypal analysis, cancer, meningioma, toxicity, visual field, radiation-induced optic neuropathy, proton therapy, modeling, artificial intelligence.

1 Introduction

Radiation therapy is a cornerstone in the treatment of many head and neck (HNC), skull base, and central nervous system (CNS) tumors. However, their proximity to critical visual structures poses a significant risk of iatrogenic injury [1]. While some radiation-induced damage to radiosensitive ocular structures like the lens frequently leads to reparable damage (e.g., cataract surgery) [2], damage to the optic nerve and chiasm, i.e. radiation-induced optic neuropathy (RION) is often irreversible and under-recognized. RION may occur from injury at multiple levels, from the retinal ganglion cell layer representing axons of the optic nerve in the retina, or the nerve fibers and myelin of the intraorbital optic nerve or chiasm and even retrochiasmal pathways in the occipital lobes [3,4] [5,6], [4,7]. Risk factors for RION include direct compression, surgical scarring, and vascular comorbidities such as hypertension and diabetes [8,9].

Conventional toxicity assessment relies primarily on visual acuity metrics, as codified by standard oncology grading systems. Yet visual acuity is insensitive to early or localized optic pathway damage, as it primarily reflects macular function. Additionally, visual acuity lacks specificity to RION as it can also be affected by cataracts, dry eye syndrome, or retinopathy [10,] [11,12]. In contrast to visual acuity testing, automated static perimetry provides a spatially resolved view of visual field sensitivity, offering a more anatomically specific window into optic nerve integrity. However, traditional perimetric outputs, such as the mean deviation, collapse this complex, high-dimensional data into a single global score, failing to capture clinically meaningful patterns of functional loss [13,14] [15,16].

To address this limitation, we propose the use of archetypal analysis, a data-driven artificial intelligence approach. This unsupervised learning method identifies a small set of representative and interpretable patterns, archetypes, that capture the principal modes of variation within high-dimensional data [16–18]. Applied to visual field perimetry, archetypal analysis enables the identification of spatially distinct visual loss patterns, reflecting underlying neuro-ophthalmologic anatomical damage. When integrated with radiation image and dose maps, this approach can reveal voxel-level, radioanatomic correlations between treatment exposure and observed toxicity. Archetypal analysis can categorize patients into specific archetypes based on their visual field defects, allowing for a more structured and interpretable understanding of visual damage patterns [16–18]. Archetypal analysis also provides a unique methodology to link semiology (e.g. clinical expression of damage), physiology and anatomy with the effects of local treatments, such as surgery and radiotherapy.

This study introduces a novel application of archetypal analysis, a data-driven artificial intelligence technique, to model the evolution of visual field deficits in a prospective cohort of patients with para-optic tumors treated using pencil beam scanning proton therapy. By linking quantitative radiation dose metrics to functional patterns of visual loss, this approach enables a more precise spatial mapping of radiation-induced damage and offers new mechanistic insights into the pathogenesis of radiation-induced optic neuropathy (RION).

2 Materials and Methods

2.1 Study Population

A prospective Institutional Review Board approved (INT-24-016 of Baclesse Cancer center) pencil beam scanning proton therapy cohort was conducted since 2018. Patients at risk of optic deterioration due to their tumor location underwent comprehensive ophthalmologic assessment (included visual field by perimetry, visual acuity by the ETRDS scale, ganglion cell layer integrity, retinal fiber thickness and vascular integrity by macular, papillary and angiographic optical coherence tomography, and optic nerve function by visual evoked potentials) at baseline (e.g. before radiotherapy, but after surgery if any) biannually for two years, and annually thereafter. This selection was performed during weekly proton therapy tumor board meetings, focusing on individuals diagnosed with para-optic CNS/skull-base/HNC tumors. Treatment was delivered in 1.8–2.2 Gy per fraction, with a median total dose of 54.0 Gy (range: 48.0–74.0 Gy).

In the context of RION, visual field loss can serve as a sensitive and functionally meaningful surrogate of toxicity. However, unlike visual acuity loss, which is graded using the Common Terminology Criteria for Adverse Events (CTCAE v5.0), there is no established standard for grading RION based on visual field data in radiation oncology. Standardized visual field deficits were prospectively performed using automated static perimetry (Metrovision Field 30). Each exam generated a 2D sensitivity map comprising 76 measurement points per eye, with light sensitivity reported in decibels (dB). To address this gap, we defined RION severity grades using the mean deviation (MD) of visual field sensitivity, following grading criteria commonly used in glaucoma [19]. Grades were assigned in 3 dB increments: grade 0 for MD > –3 dB (normal or near-normal field), grade 1 for –3 to –6 dB, grade 2 for –6 to –9 dB, grade 3 for –9 to –12 dB, and grade 4 for MD < –12 dB (severe loss). All visual field measurements used in this study were already age-corrected according to standard perimetry procedures. Thus, age-related visual sensitivity decline was inherently adjusted, and the observed temporal trends primarily reflect radiation-induced changes rather than natural aging effects. The grading classification allowed us to standardize and quantify the severity of visual field loss across patients and timepoints, enabling structured modeling of RION severity and its relationship to radiation exposure.

Tumor and organ-at-risk (OAR) delineation were carried out using high-resolution millimetric computed tomography (CT) scans, integrated with the RayStation Treatment Planning System (RaySearch®). Dose calculations were conducted using a Monte Carlo algorithm and accounted for a relative biological effectiveness (RBE) factor of 1.1. Radiotherapy was delivered using pencil beam scanning (PBS) proton beam therapy.

Clinical data collection included demographic details such as age and sex, metabolic and vascular conditions including diabetes, hypercholesterolemia, hypertension and smoking history. Treatment-related variables encompassed the number of surgeries, use of concomitant chemotherapy, and tumor control status, categorized as stable disease, partial response, complete response, or progressive disease/recurrence at last follow-up. Distances between the clinical target volume (CTV) and optic OARs were also measured.

2.2 Archetypal and modeling analysis

The general workflow of analysis is illustrated in Figure 1. First, archetypal analysis was applied to characterize the different damage patterns from visual field perimetry data. Then, modeling was applied to quantify the evaluation of the damage pattern over time after PBS proton therapy.

2.2.1 Archetypal Analysis

Archetypal analysis is an unsupervised machine learning technique that approximates each data point as a convex combination of extremal points called archetypes, and those archetypes are themselves convex combinations of the original data points. In archetypal analysis, the dataset is represented as a matrix $X \in \mathbb{R}^{n \times p}$, where n is the number of observations and p is the number of features. Archetypes (Z) are defined as convex combinations of data points:

$$Z = X^T \beta \; with \; \beta_{ij} \geq 0 \; and \; \sum_j \beta_{ij} = 1$$

where β_{ij} is the weight of the i-th data point in forming the j-th archetype ($\beta \in \mathbb{R}^{k \times n}$; $Z \in \mathbb{R}^{p \times k}$). Each observation is then approximated by a convex combination of these archetypes:

$$\hat{X} = \alpha Z \; with \; \alpha_{ij} \geq 0 \; and \; \sum_j \alpha_{ij} = 1$$

where α_{ij} is the weight of the j-th archetype in approximating the i-th observation ($\alpha \in \mathbb{R}^{n \times k}$). The objective is to minimize the reconstruction error, quantified by the residual sum of squares (RSS):

$$\min_{\alpha, \beta} \|Z - \alpha Z\|_F^2$$

Archetypal analysis was performed separately by eye and by individual, using the archetypes package (version 2.2.0.1) in RStudio. The optimal number of archetypes was defined as the minimal number of archetypes corresponding to clinically relevant visual field patterns (difference between residual sum of square between two consecutives number of archetypes lower than 0.01).

Archetypal Analysis by Eye

Eye-based analysis was analyzed based on 76 measurement points per eye from each patient. Data exploration involved evaluating archetypal proportion evaluation over time to identify distinct visual field deficit patterns. Visual field perimetry assessed light sensitivity deficits in decibels (dB) pre- and post-radiotherapy at 6 and 12 months, followed by annual evaluations.

To assess the correlation between dose and changes in archetypal proportions, the proportion of each archetype for each eye of each patient was fitted with a linear regression model. The rate of change of the proportions was calculated post-radiotherapy. Correlations were examined with the minimum, mean, and maximum doses delivered to the retina, optic nerve, and chiasma. The analysis was stratified by baseline visual field deficits, and the correlation coefficients were computed to determine how radiation doses to the organs-

at-risk influenced changes in visual damage patterns. Patients were also stratified by baseline visual field deficit into four groups: > -3 dB, -3 to -6 dB, -6 to -12 dB, and < -12 dB.

Archetypal Analysis by Individual

Individual-based analysis was analyzed based on 152 measurement points of their two eyes (or single eye for monophthalmic individuals). Baseline damage was defined as higher than 50% of the archetypal proportion of normal archetype. Transitions between archetypes over time were examined using Directed Acyclic Graph (DAG) analysis, which represents and analyzes shifts between different states in the dataset. Transition relationships were identified chronologically, and transition weights were calculated based on their frequency. Patients were then annotated by their maximum archetypal proportion at each timepoint.

2.2.2 Modeling the evaluation of archetypal proportion by time

Longitudinal changes in archetypal proportions were evaluated over a 5-year period post-radiotherapy. Changes in archetype proportions over time were analyzed using linear regression and visualized using step plots. Further stratification by tumor type (meningioma, pituitary adenoma, other CNS/skull base tumors, sinonasal tumors, other HNC) was performed to assess baseline and post-radiotherapy damage patterns.

The kinetics of archetypal proportion changes following radiotherapy were modeled in patients with no (0; -3dB) or minor (-3; -6 dB) deficits at baseline. Patients with baseline deficit, defined by a MD worse than -6 dB, and related ocular disease rather than RION before or/and after radiotherapy were excluded from the analysis. Timepoints were standardized across patients (e.g., 0, 0.5, 1, 2, 3, 4, and 5 years), and missing timepoints were imputed using last observation carried forward (LOCF). A linear regression model was used to estimate the rate of change of each archetype's proportion over time.

Dosimetric parameters for the retinas, optic nerves, and optic chiasma were extracted from radiotherapy plans, including minimum, mean, and maximum doses. Correlation between dose parameters and the rate of change in archetype proportions was assessed using Pearson’s correlation coefficients. Analyses were stratified by baseline visual field deficit severity.

2.2.3 Statistical analysis

All statistical analyses were performed using R (version 4.2), with statistical significance set at p-value < 0.05. Statistical comparisons between groups were conducted using Student’s t-test for normally distributed continuous variables and the Mann–Whitney U test for non-normally distributed data. Chi-square and Fisher’s exact tests were applied for categorical variables. Correlation analyses between archetypal proportions, time after radiotherapy, and dose metrics were performed using Spearman correlation coefficients. Temporal changes in archetypal dynamics were further evaluated using linear mixed-effects models.

3 Results

The cohort consisted of 236 patients for the archetypal analysis. The median age was 60.1 years (range: 17.5-90.6), with 93 males and 143 females. Tumors included 155 CNS cases (81 meningiomas, 36 pituitary adenomas, 11 craniopharyngiomas, 27 others) and 81 HNC cases (56 sinonasal tumors, 25 others). The median deficit was -1.3 dB (range: -12.3 to 1.5) at baseline. Details of patient characteristics and treatment are reported in Table 1.

3.1 Archetypal Analysis by Eye

The optimal number of visual field archetypes was 10 (Figure S1) at baseline, including tunnel vision, nasal-superior quadrantanopia, full-eye damage, temporal-superior quadrantanopia, temporal hemianopia, nasal-inferior quadrantanopia, peripheral scotoma, and dermatochalasis. In addition, there were two archetypes that corresponded to a normal visual field pattern (Figure 2A). The peripheral scotoma archetype was considered artefactual (related to technical acquisition including errors in the visual field measuring procedure, such as improper fixation or other acquisition-related artifacts), and the dermatochalasis archetype was artefactual due to physiological ptosis [20]. Normal, peripheral scotoma and dermatochalasis were therefore grouped into a normal archetype category, resulting in 7 archetypes retained for analyses.

The temporal evolution of archetypal visual field patterns following radiotherapy was analyzed, with data stratified by baseline MD in 3 dB increments (Figure 2B). Among patients with a baseline MD greater than -3 dB, the proportion of the normal visual field archetype declined at a rate of 1.9% per year ($p < 0.001$), while the prevalence of abnormal archetypes gradually increased. In patients with a baseline MD between -3 and -6 dB, the normal archetype decreased more rapidly, at 9.7% per year ($p < 0.001$), accompanied by a corresponding rise in abnormal patterns. In groups with baseline MD between -6 and -9 dB or -9 and -12 dB, the normal archetype initially increased during the first two years post-radiotherapy, followed by a subsequent decline (reduction rate per year as 1.88%, $p = 0.44$ and 4.90%, $p = 0.03$, respectively). Interestingly, patients with severe baseline deficits (MD < –12 dB) showed a progressive increase rate of 11.9% per year in the proportion of the normal archetype over time ($p < 0.001$), while the proportion of archetypes representing full-field visual loss decreased at the rate of 15.4% per year ($p < 0.001$).

Visual field damage patterns varied by tumor type both at baseline and following radiotherapy (Figure 2C). At baseline, patients with meningiomas and pituitary adenomas exhibited a higher proportion of full-field visual loss and temporal superior quadrantanopia compared to other CNS tumors. Pituitary adenomas were additionally associated with a slightly higher frequency of nasal inferior quadrantanopia, while meningiomas showed a more evenly distributed spectrum of visual field deficits. Other CNS/skull base tumors were associated with moderate visual impairment, characterized by a greater prevalence of tunnel vision and temporal hemianopia. HNC rarely resulted in significant visual field damage, with only a small proportion of cases demonstrating detectable impairment.

At follow-up after radiotherapy, for patients with no baseline visual deficits (mean deficit greater than -3 dB), the changes over time were minimal. In patients with minor baseline deficits (mean deficit between -6 and -3 dB), the reduction of normal archetypes was more pronounced in meningioma patients, where the majority of visual deficits manifested as full eye damage and tunnel vision. For patients with significant baseline damage (mean deficit lower than -6 dB, especially below -12 dB), there was evidence of recovery after radiotherapy, reflected in an increase in the proportion of patients showing no visual damage. In pituitary adenomas and other CNS/skull base tumors, occurrence and subsequent increase was observed in the proportion of temporal superior quadrantanopia and temporal hemianopia. In sinonasal HNC, tunnel vision was the predominant form of visual damage. For other HNC, a high proportion of patients with pre-existing visual field deficits at baseline developed nasal superior and inferior quadrantanopia.

The rate of change in archetypal proportions over time was analyzed in relation to the dose received by organs-at-risk, specifically the retinas, optic nerves, and chiasma.

In patients without baseline visual field damage (MD > -3 dB), the rate of decline in the “normal” archetype was negatively correlated with both the mean and minimum doses to the optic chiasma ($p < 0.001$). Similarly, the progression of the “nasal superior quadrantanopia” archetype was negatively correlated with chiasma dose ($p = 0.022$ and $p = 0.003$ for average and maximum dose, respectively). In patients with mild baseline deficits (MD between –6 and –3 dB), the rate of increase in the “full eye damage” archetype was positively correlated with both the mean and minimum doses to the optic nerve ($p < 0.001$, and $p = 0.002$ for minimum and average dose, respectively) and retina ($p < 0.01$ for minimum and average dose, and $p = 0.009$ for maximum dose).

In patients with a baseline mean deviation between -9 and -6 dB, the rate of change of the “normal” archetype was negatively correlated with both the mean and minimum doses to the retina ($R = -0.5$ to -0.6, $p = 0.03$ and 0.01, respectively). Conversely, the rate of change of the “full eye damage” archetype showed a positive correlation with these same dose metrics ($p = 0.004$, $p < 0.001$, and $p = 0.001$ for minimum, average, and maximum dose to the retina, respectively). The distance between the tumor and the optic nerve or chiasma was positively correlated with the expression of the “temporal hemianopia” archetype ($p < 0.001$).

In patients with a baseline mean deviation between -12 and -9 dB, the rate of change of the “tunnel vision” archetype was negatively correlated with retinal dose ($p = 0.050$). The change rate of the “temporal hemianopia” archetype was also negatively correlated with dose to the optic chiasma ($p < 0.001$, $p = 0.003$, and $p = 0.018$ for minimum, average, and maximum dose, respectively). In contrast, the rate of change of the “nasal inferior quadrantanopia” archetype was positively correlated with the minimum dose to the retina ($p = 0.001$). For patients with severe baseline damage (MD<-12 dB), no significant correlations were found (Figure 3).

3.2 Archetypal Analysis by Individual

Nine archetypes were identified at the individual level (Figure S2), with patients grouped into normal, tunnel vision, bi-temporal hemianopia, full-eye damage, and superior quadrantanopia (Figure 4A). For tunnel vision,

bi-temporal hemianopia, and superior quadrantanopia, both eyes were affected together. For full-eye damage, damage occurred on a single side (either left or right).

In individuals with normal MD at baseline, the normal archetype decreased over time, whereas those with major damage at baseline had an increased proportion of normal archetype after radiotherapy (Figure 4B). Among patients with normal MD at baseline (n=147, with 111 having follow-up data), the majority (n=102) maintained their normal archetype status after radiotherapy. However, 9 patients transitioned to full-eye damage, tunnel vision, or bi-temporal hemianopia within a year post-radiotherapy. One patient transitioned to superior quadrantanopia before eventually developing full-eye damage. In the group with full-eye damage at baseline (n=26, with 12 having follow-up data), five initially recovered to normal after radiotherapy but later redeveloped full-eye damage. Patients in the tunnel vision baseline group (n=7, with 4 follow-up cases) exhibited varied responses, with one recovering to normal and two progressing to full-eye damage. Among patients (n=4) with baseline bi-temporal hemianopia, patients either remained in the same category or developed full-eye damage or tunnel vision. The single patient presenting with superior quadrantanopia at baseline showed no change in visual field status following radiotherapy (Figure 4C).

3.3 Temporal Modeling of Archetypal Proportion Dynamics

The analysis included 255 eyes from 134 patients (Figure 1) who had no/minor visual deficits at baseline (MD > -6 dB), having at least 1 follow-up point, and no related ocular condition at baseline or after radiotherapy. The cohort was made of 67 males and 67 females, median age 57.8 years old (range: 17.6–89.5). At baseline, the median mean deficit was -0.8 dB (range: -5.5 to 1.5). The median minimum, mean, and maximum radiation doses to the optic nerve were 2.5 Gy, 26.7 Gy, and 51.4 Gy, respectively. For the optic chiasma, the corresponding values were 36.1 Gy, 45.2 Gy, and 50.7 Gy. The retina received substantially lower doses, with median minimum, mean, and maximum values of 0.1 Gy, 1.3 Gy, and 7.8 Gy, respectively. The median follow-up duration was 23.2 months (range: 3.5–59.8 months) after radiotherapy.

Archetype proportion was significantly correlated with time after radiotherapy in all archetypal groups but the nasal-superior damage (Figure 5). The normal archetype proportion declined by 1.9% per year ($p < 0.001$). Damage patterns increased at various rates: full-eye damage by 0.6% ($p < 0.001$), tunnel vision by 0.3% ($p = 0.006$), temporal damage by 0.6% ($p < 0.001$), superior temporal damage by 0.2% ($p = 0.023$), and nasal-inferior damage by 0.1% per year ($p = 0.035$).

Correlation analysis of archetypal proportion with time after radiotherapy and dose to the optic nerves, optic chiasma, and retinas classified damage patterns into three clusters (Figure S4). The first cluster, associated with the retinal and optic nerve minimum dose, was negatively correlated with the normal archetype and positively correlated with nasal-inferior damage. The second cluster, which included the optic chiasma and optic nerve maximum dose, negatively correlated with the normal archetype but positively correlated with temporal,

temporal-superior, and full-eye damage. The third cluster, characterized by the optic nerve mean dose, was also negatively correlated with the normal archetype.

4 Discussion

Our study highlights the potential of archetypal analysis as a tool to identify archetypal patterns of visual field loss related to the location of the optic nerve or chiasma damage, in particular after radiotherapy using scanned proton beams. By identifying and tracking distinct patterns of visual field damage, we identified distinct visual field loss maps, i.e. archetypes, representative of tumor location and radiation dose. We were able to further study associated risk factors, and dose-response relationships. These findings provide a new perspective in evaluating RION in space and time, and reconnect patient perception with damage along the optic pathways, therefore complementing traditional binary RION endpoints.

Archetypal analysis has been previously used to study visual field changes in optic neuropathies including glaucoma [21–23], papilledema from idiopathic intracranial hypertension [24], and optic neuritis [25]. While the correlation between anatomical location and visual field damage is well-documented in optic neuropathies such as glaucoma and optic neuritis, it is hardly characterized in the oncology context and to understand radiation damage. Our study expands the scope of archetypal analysis by applying it to RION, a condition where visual outcomes can vary widely and may include both deterioration and partial recovery.

In patients with moderate-to-severe baseline visual field loss (mean deviation between –12 and –9 dB), changes in specific visual field patterns over time were linked to radiation dose at anatomically relevant sites. A higher dose to the retina was associated with a slower increase of the “tunnel vision” archetype, suggesting that retinal injury may limit the progression or expression of this diffuse damage pattern. Similarly, higher radiation dose to the optic chiasma was associated with a reduced progression of the “temporal hemianopia” archetype, which anatomically corresponds to crossing nasal fibers from both eyes that converge at the chiasma. In contrast, increased dose to the retina was linked to a greater expression of the “nasal inferior quadrantanopia” archetype, a localized pattern consistent with damage to the superior temporal retinal regions. These findings suggest that dose-dependent injury to specific segments of the optic apparatus leads to distinct and anatomically coherent visual field patterns, which archetypal analysis can capture and quantify over time. The identified archetypes are consistent with the known anatomy of the visual pathways. For instance, monocular visual loss typically reflects disease of the eyeball or optic nerve in its intraconal portion [26], while bilateral visual loss—including homonymous hemianopia—suggests a lesion at or posterior to the optic chiasm [26]. Bitemporal hemianopia is commonly associated with chiasmal damage caused by tumors or lesions impinging on the optic chiasm [27]. RION may present with a combination of different visual field damage types, complicating characterization and reinforcing the utility of archetypal analysis. As an unsupervised machine learning technique, archetypal analysis is suited to analyze complex and heterogeneous datasets [28], such as those generated by visual field testing in patients with varying degrees and patterns of optic nerve damage.

Furthermore, the pattern of visual field damage varied according to tumor type and location, which aligns with known anatomical relationships. Tumor type is often related to the size and position of the tumor and, in turn, influences the extent and nature of radiation-induced damage to nearby organ-at-risks. In addition, the observed dose–response relationships support and extend existing radiation tolerance models. The correlation between visual deficit and radiation dose to optic structures builds upon traditional dose-volume studies [4,7,29,30]. However, our findings introduce a pattern-based perspective that enhances our understanding of radiation-induced damage beyond standard models, which typically focus on visual acuity as the primary endpoint. By incorporating archetypal patterns into dose–response assessments, we can detect spatial changes in visual field loss that may not be captured through conventional metrics.

Our observation showed that patients with better baseline visual function experienced slower deterioration in comparison to those with moderate baseline deficits, suggesting that initial damage may accelerate RION progression. Conversely, patients with severe deficits at baseline sometimes showed stabilization or even improvement after radiotherapy. This finding is consistent with previous studies indicating that early deficits, particularly those caused by compressive or inflammatory mechanisms, may be at least partially reversible [31,32]. Improvements in visual function may reflect positive treatment responses, such as tumor shrinkage relieving pressure on the chiasm or optic nerves.

Study limitations include the presence of confounding ocular disorders such as glaucoma, amblyopia, or diabetic retinopathy, which may add noise to the analyses of visual outcomes. However, the fact that analyses were performed with adjustment on baseline status and the timescale of the study minimize this risk. Additionally, despite being the largest cohort to date in this field, the sample size and follow-up duration remain modest. Late-onset RION may not have been fully captured, and loss to follow-up could introduce biases in longitudinal analyses. Future studies should aim to validate our findings across larger, multicenter cohorts with extended follow-up. Integrating other examinations to access RION at the mechanistic level (e.g., optical coherence tomography, visual evoked potential, or other structural imaging modalities) may also enhance the understanding of the relationship between radiation dose, structural damage, and functional loss.

In conclusion, our findings offer a foundation for a paradigm shift in the evaluation and management of RION, one that is pattern-based, functionally driven, and tailored to individual risk profiles. Archetypal analysis provides a pattern-based and functionally driven framework to study spatially distinct visual field loss, complementing conventional binary or acuity-based endpoints. While exploratory, this approach may support future voxel-based dose–outcome modeling and, when integrated with LET, dose-rate, and planning parameters, could eventually inform more data-driven personalization of radiotherapy strategies.

References

1. Brook I. Late side effects of radiation treatment for head and neck cancer. *Radiat Oncol J*. 2020;38(2):84-92. doi:10.3857/roj.2020.00213

2. Ainsbury EA, Dalke C, Hamada N, et al. Radiation-induced lens opacities: Epidemiological, clinical and experimental evidence, methodological issues, research gaps and strategy. *Environment International*. 2021;146:106213. doi:10.1016/j.envint.2020.106213

3. Danesh-Meyer HV. Radiation-induced optic neuropathy. *Journal of Clinical Neuroscience*. 2008;15(2):95-100. doi:10.1016/j.jocn.2007.09.004

4. Ozkaya Akagunduz O, Guven Yilmaz S, Yalman D, et al. Evaluation of the Radiation Dose–Volume Effects of Optic Nerves and Chiasm by Psychophysical, Electrophysiologic Tests, and Optical Coherence Tomography in Nasopharyngeal Carcinoma. *Technol Cancer Res Treat*. 2017;16(6):969-977. doi:10.1177/1533034617711613

5. Grosinger A, Chen JJ, Link MJ, Bhatti MT. Detection of Asymptomatic Radiation Induced Optic Neuropathy with Optical Coherence Tomography. *Neuroophthalmology*. 2021;45(5):339-342. doi:10.1080/01658107.2020.1871031

6. Lecornu M, Lesueur P, Salleron J, et al. Prospective Assessment of Early Proton Therapy-Induced Optic Neuropathy in Patients With Intracranial, Orbital or Sinonasal Tumors: Impact of A Standardized Ophthalmological Follow Up. *Front Oncol*. 2021;11:673886. doi:10.3389/fonc.2021.673886

7. Mayo C, Martel MK, Marks LB, Flickinger J, Nam J, Kirkpatrick J. Radiation Dose–Volume Effects of Optic Nerves and Chiasm. *International Journal of Radiation Oncology*Biology*Physics*. 2010;76(3):S28-S35. doi:10.1016/j.ijrobp.2009.07.1753

8. Delanian S, Lefaix JL, Pradat PF. Radiation-induced neuropathy in cancer survivors. *Radiotherapy and Oncology*. 2012;105(3):273-282. doi:10.1016/j.radonc.2012.10.012

9. Köthe A, Van Luijk P, Safai S, et al. Combining Clinical and Dosimetric Features in a PBS Proton Therapy Cohort to Develop a NTCP Model for Radiation-Induced Optic Neuropathy. *International Journal of Radiation Oncology*Biology*Physics*. 2021;110(2):587-595. doi:10.1016/j.ijrobp.2020.12.052

10. Freites-Martinez A, Santana N, Arias-Santiago S, Viera A. CTCAE versión 5.0. Evaluación de la gravedad de los eventos adversos dermatológicos de las terapias antineoplásicas. *Actas Dermo-Sifiliográficas*. 2021;112(1):90-92. doi:10.1016/j.ad.2019.05.009

11. Matsuura M, Hirasawa K, Murata H, Asaoka R. The Relationship Between Visual Acuity and the Reproducibility of Visual Field Measurements in Glaucoma Patients. *Invest Ophthalmol Vis Sci*. 2015;56(9):5630. doi:10.1167/iovs.15-17576

12. Asaoka R, Miyata M, Oishi A, et al. Relationship between visual acuity and visual field and its reproducibility in patients with retinitis pigmentosa. *Eye*. 2023;37(6):1094-1099. doi:10.1038/s41433-022-02043-0

13. Strouthidis NG, Vinciotti V, Tucker AJ, Gardiner SK, Crabb DP, Garway-Heath DF. Structure and Function in Glaucoma: The Relationship between a Functional Visual Field Map and an Anatomic Retinal Map. *Invest Ophthalmol Vis Sci*. 2006;47(12):5356. doi:10.1167/iovs.05-1660

14. Tao A, Liang Y, Chen J, et al. Structure-function correlation of localized visual field defects and macular microvascular damage in primary open-angle glaucoma. *Microvascular Research*. 2020;130:104005. doi:10.1016/j.mvr.2020.104005

15. Artes PH, Nicolela MT, LeBlanc RP, Chauhan BC. Visual Field Progression in Glaucoma: Total Versus Pattern Deviation Analyses. *Invest Ophthalmol Vis Sci*. 2005;46(12):4600. doi:10.1167/iovs.05-0827

16. Branco J, Elze T, Wang JK, et al. Longitudinal visual field archetypal analysis of optic neuritis treated in a clinical setting. *BMJ Open Ophth*. 2022;7(1):e001136. doi:10.1136/bmjophth-2022-001136

17. Solli E, Doshi H, Elze T, et al. Archetypal analysis of visual fields in optic neuritis reveals functional biomarkers associated with outcome and treatment response. *Multiple Sclerosis and Related Disorders*. 2022;67:104074. doi:10.1016/j.msard.2022.104074

18. Branco J, Elze T, Wang JK, et al. Archetypal analysis of longitudinal visual fields for idiopathic intracranial hypertension patients presenting in a clinic setting. Liu N, ed. *PLOS Digit Health*. 2023;2(5):e0000240. doi:10.1371/journal.pdig.0000240

19. Susanna Jr. R, Vessani RM. Staging Glaucoma Patient: Why and How? *TOOPHTJ*. 2009;3(2):59-64. doi:10.2174/1874364100903020059

20. Heijl A, Åsman P. Pitfalls of automated perimetry in glaucoma diagnosis: Editorial review: *Current Opinion in Ophthalmology*. 1995;6(2):46-51. doi:10.1097/00055735-199504000-00008

21. Cai S, Elze T, Bex PJ, Wiggs JL, Pasquale LR, Shen LQ. Clinical Correlates of Computationally Derived Visual Field Defect Archetypes in Patients from a Glaucoma Clinic. *Current Eye Research*. 2017;42(4):568-574. doi:10.1080/02713683.2016.1205630

22. Elze T, Pasquale LR, Shen LQ, Chen TC, Wiggs JL, Bex PJ. Patterns of functional vision loss in glaucoma determined with archetypal analysis. *J R Soc Interface*. 2015;12(103):20141118. doi:10.1098/rsif.2014.1118

23. Wang M, Tichelaar J, Pasquale LR, et al. Characterization of Central Visual Field Loss in End-stage Glaucoma by Unsupervised Artificial Intelligence. *JAMA Ophthalmol*. 2020;138(2):190. doi:10.1001/jamaophthalmol.2019.5413

24. Doshi H, Solli E, Elze T, Pasquale LR, Wall M, Kupersmith MJ. Unsupervised Machine Learning Identifies Quantifiable Patterns of Visual Field Loss in Idiopathic Intracranial Hypertension. *Trans Vis Sci Tech*. 2021;10(9):37. doi:10.1167/tvst.10.9.37

25. Solli E, Doshi H, Elze T, Pasquale L, Wall M, Kupersmith M. Archetypal Analysis Reveals Quantifiable Patterns of Visual Field Loss in Optic Neuritis. *Trans Vis Sci Tech*. 2022;11(1):27. doi:10.1167/tvst.11.1.27

26. Callard J, Kilmark J, Mohamed H. Ocular Emergencies. *Physician Assistant Clinics*. 2017;2(3):519-536. doi:10.1016/j.cpha.2017.02.014

27. Yoshihara MK, Lui F. Neuroanatomy, Bitemporal Hemianopsia. In: *StatPearls*. StatPearls Publishing; 2023. https://www.ncbi.nlm.nih.gov/books/NBK545213/

28. Cutler A, Breiman L. Archetypal analysis. *Technometrics*. 1994;36(4):338-347.

29. Moiseenko V, Song WY, Mell LK, Bhandare N. A comparison of dose-response characteristics of four NTCP models using outcomes of radiation-induced optic neuropathy and retinopathy. *Radiat Oncol*. 2011;6:61. doi:10.1186/1748-717X-6-61

30. Wu YL, Li WF, Yang KB, et al. Long-Term Evaluation and Normal Tissue Complication Probability (NTCP) Models for Predicting Radiation-Induced Optic Neuropathy after Intensity-Modulated Radiation Therapy (IMRT) for Nasopharyngeal Carcinoma: A Large Retrospective Study in China. Xu Y, ed. *Journal of Oncology*. 2022;2022:1-10. doi:10.1155/2022/3647462

31. Deng MY, Rauh S, Anil G, et al. Analysis of safety and efficacy of proton radiotherapy for optic nerve sheath meningioma. *Neuro-Oncology Advances*. 2024;6(1):vdae160. doi:10.1093/noajnl/vdae160

32. Paulsen F, Doerr S, Wilhelm H, Becker G, Bamberg M, Claßen J. Fractionated Stereotactic Radiotherapy in Patients With Optic Nerve Sheath Meningioma. *International Journal of Radiation Oncology*Biology*Physics*. 2012;82(2):773-778. doi:10.1016/j.ijrobp.2010.11.018

Figures

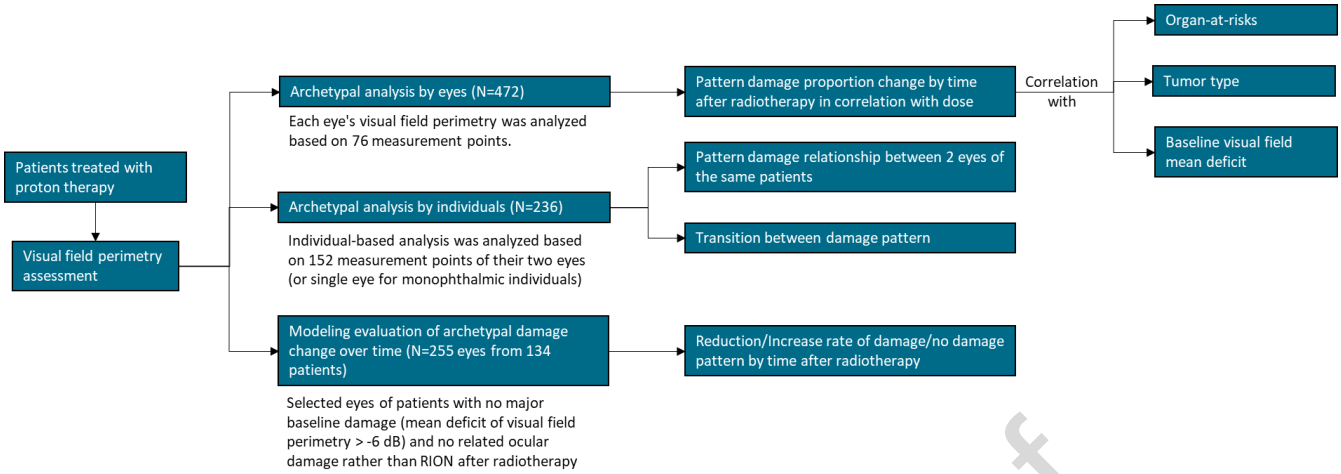

Figure 1. Workflow for archetypal and modeling analysis of optical damage pattern evaluation after radiotherapy.

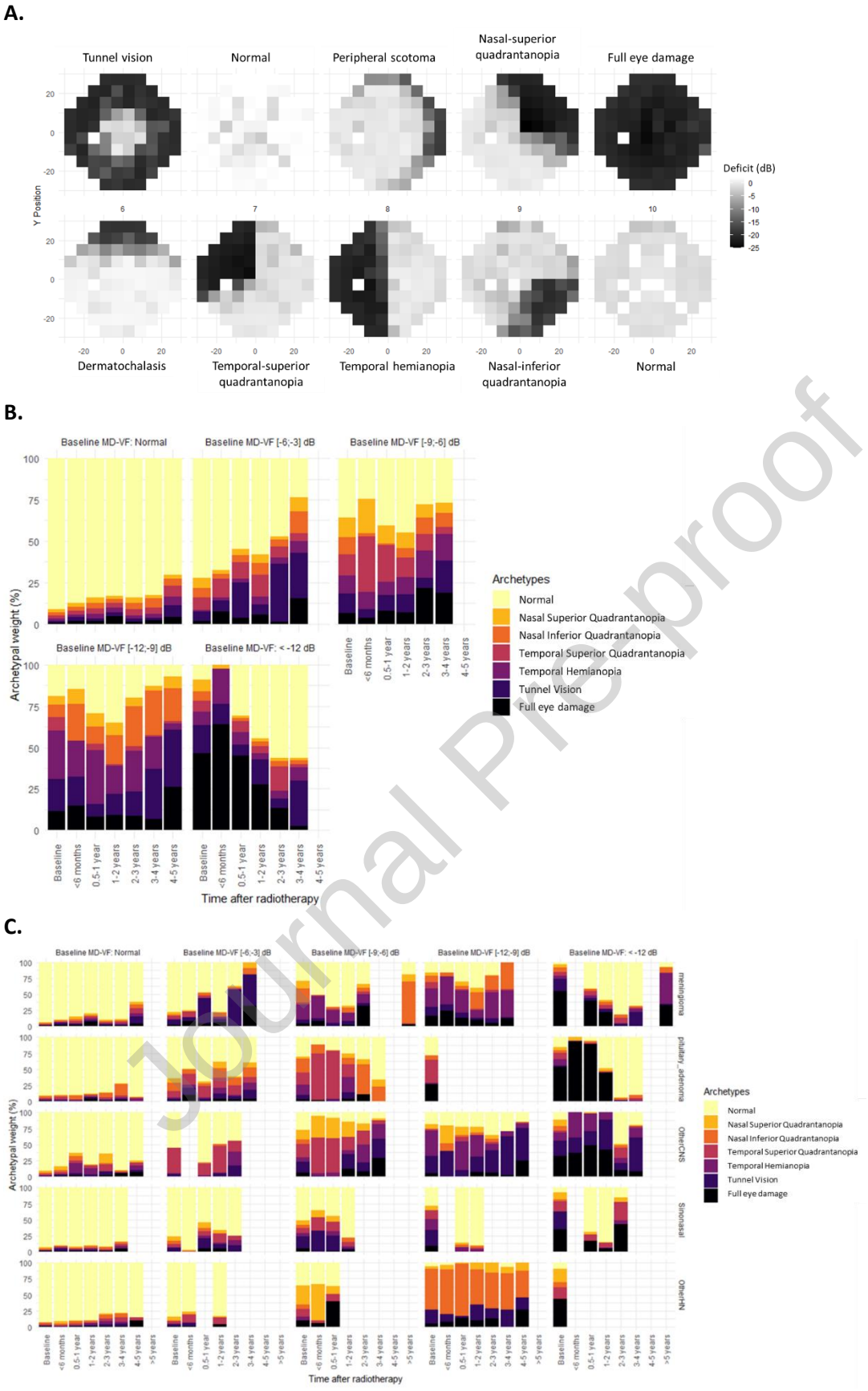

Figure 2. Analysis of archetype by eye: (A) archetypes classification; (B) archetypal longitudinal evolution after radiotherapy of the whole population stratified by baseline mean deficit of the visual field perimetry; and (C) Archetypal proportions of visual damage evaluation after radiotherapy stratified by tumor types.

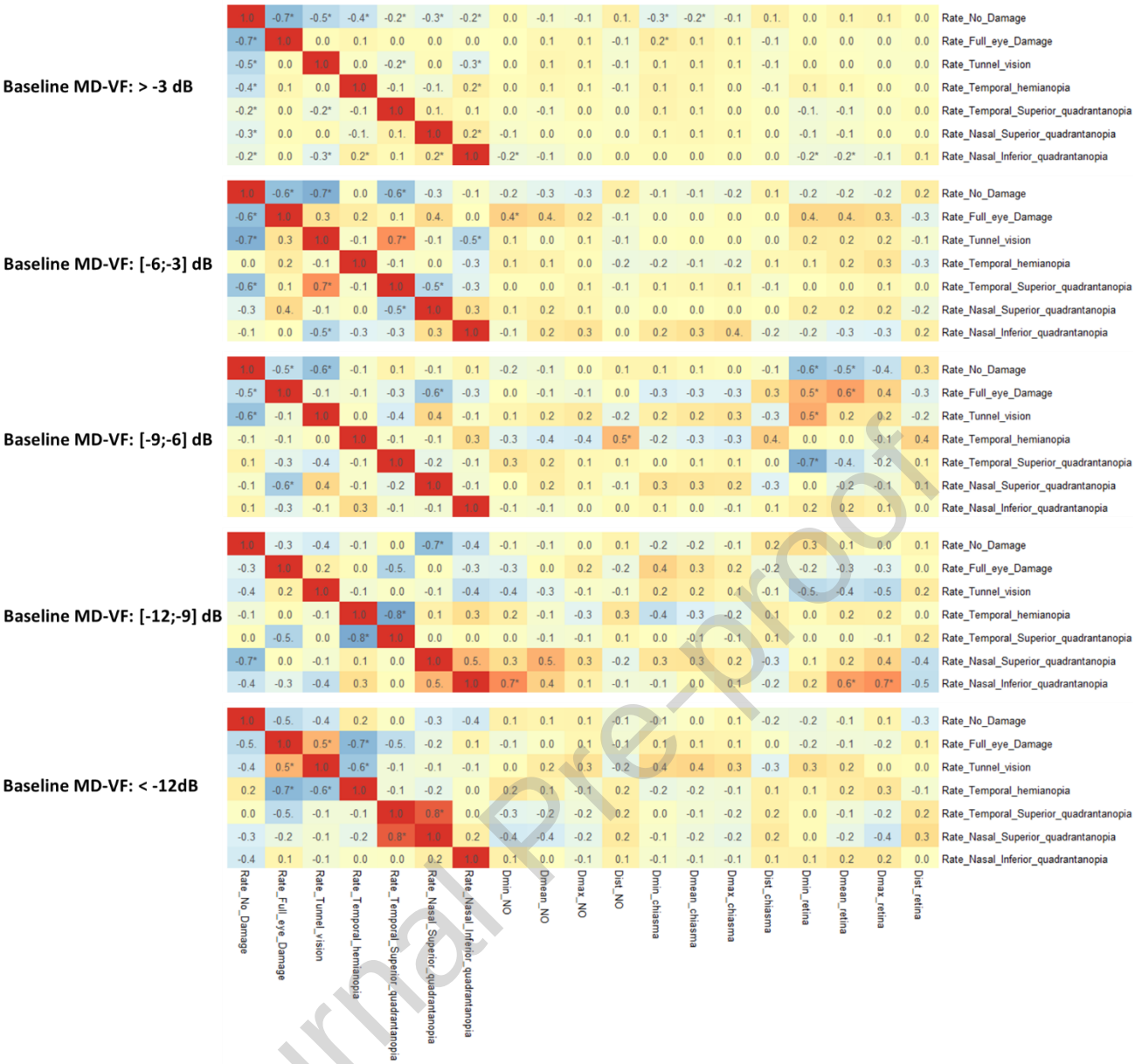

Figure 3. Rate change of archetypal proportion by time in correlation with dose to the organ-at-risk, stratified by mean deficit of visual field perimetry at baseline.

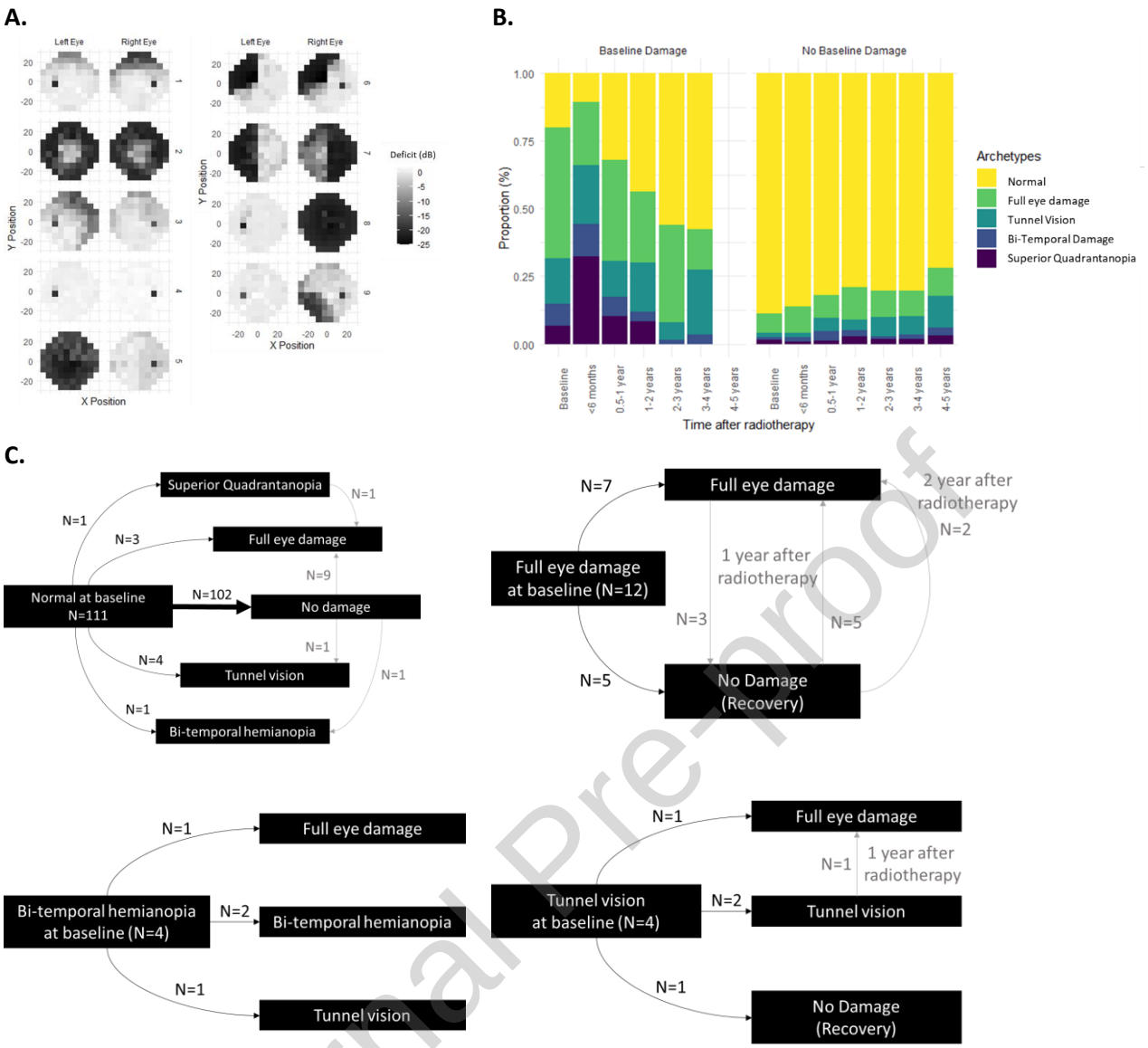

Figure 4. Archetype by individual: (A) Archetype classification; (B) Archetypal longitudinal evolution after radiotherapy of the whole population stratified by baseline archetype; (c) Transition analysis between archetypal group by time. For superior quadrantanopia, there is no evaluation by time.

Legend: Baseline damage was defined as higher 50% of the archetypal proportion of normal archetype.

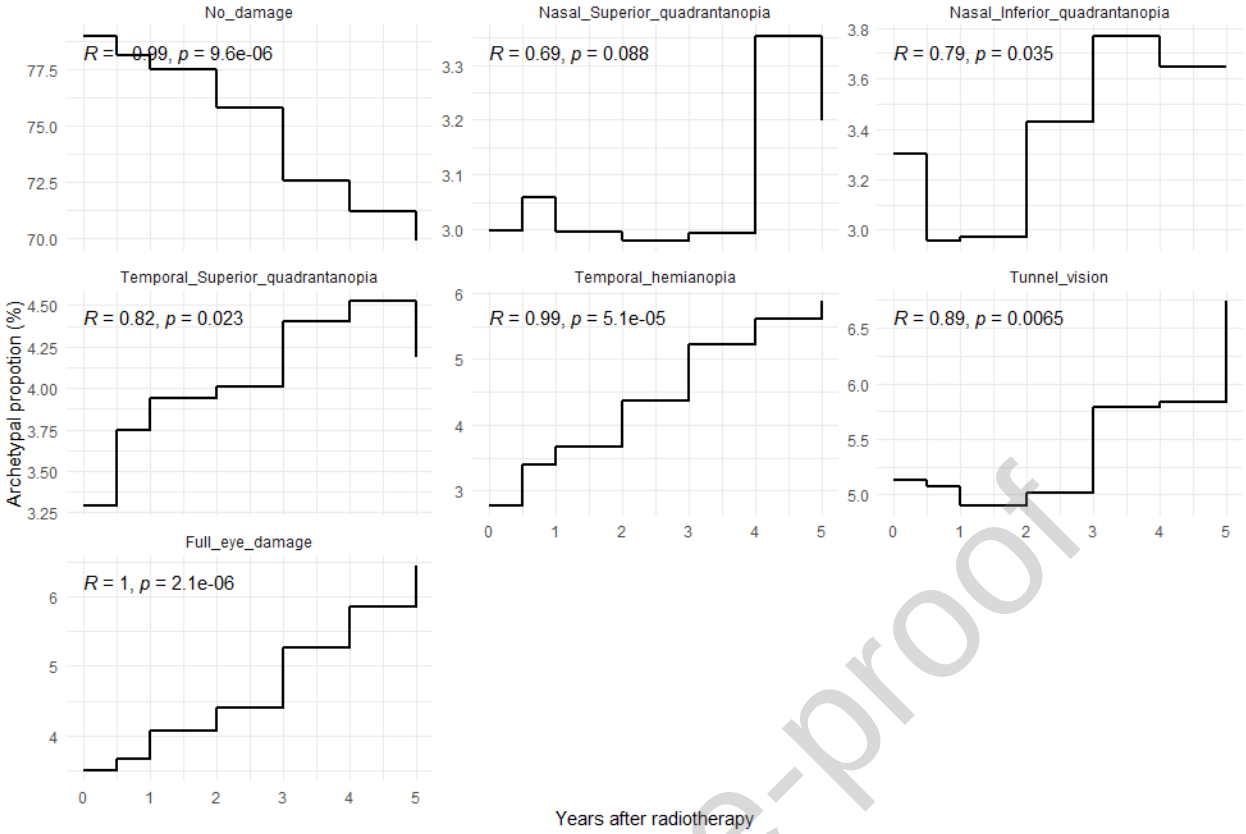

Figure 5. Longitudinal analysis of archetype evolution after radiotherapy in individuals with normal MD at baseline.

Tables

Table 1. Patients and treatment characteristics

Category	Data
Median Age (Years, Range)	60.1 (17.5-90.6)
Sex Distribution	93 Males, 143 Females
Tumor Types (Patients)	CNS Tumors (N=155) - Meningiomas (N=81) - Pituitary Adenomas (N=36) - Craniopharyngioma (N=11) - Other CNS Tumors (N=27) HNC Tumors (N=81) - Sinonasal Tumors (N=56) - Other HNC Tumors (N=25)
Comorbidities (Patients, %)	Hypertension (68, 28.5%) Diabetes (27, 11.3%) High Cholesterol (51, 21.0%) Smoking History (62, 26.0%)
Surgical History (Patients, %)	No Surgery: 81 (33.9%) 1 Surgery: 95 (39.9%) ≥2 Surgeries: 62 (26.0%)
Concomitant Chemotherapy	22 Patients (9.2%)
Median Baseline Visual Acuity	>20/40: 316 Eyes (70.8%); Between 20/40 and 20/200: 26 Eyes (5.8%) < 20/200: 29 eyes (6.5%) Missing baseline data: 75 eyes (16.8%)
Median Baseline visual field deficit (dB, Range)	- 1.3 (-21.3 to 1.5) Higher than -3 dB: 263 eyes (58.9%) Higher than -6 dB and lower than -3 dB: 47 eyes (10.5%) Higher than -9 dB and lower than -6 dB: 30 eyes (6.7%) Higher than -12 dB and lower than -9 dB: 21 eyes (4.7%) Lower than -12 dB: 38 eyes (8.5%) Missing baseline data: 47 eyes (10.5%)
Median Optic Disc Follow-up (Months, Range)	12.4 (0.3-59.8)
Median Follow-up (Living Patients, Months, Range)	43.2 (2.4-74.4)
Dead at Last Follow-up	35 Patients (14.7%)

Declaration of Interest Statement

The authors declare no conflicts of interest.